SUPPLEMENTAL MATERIAL

A ternary heterogeneous hydrogel with strength elements for resilient, self-healing, and recyclable epidermal electronics

Ziya Wang [1,2], Xiuru Xu [1], Yingtian Xu [2], Waner Lin [3], Zhengchun Peng [1,*]

[1] Center for Stretchable Electronics and Nano Sensors, School of Physics and Optoelectronic Engineering, Shenzhen University, Shenzhen 518060, China

[2] Shenzhen Institute of Artificial Intelligence and Robotics for Society (AIRS), Shenzhen 518129, China

[3] Department of Micro-Nano Electronics, School of Electronic Information and Electrical Engineering, Shanghai Jiao Tong University, Shanghai 200240, China

* Corresponding author. E-mail addresses: zcpeng@szu.edu.cn

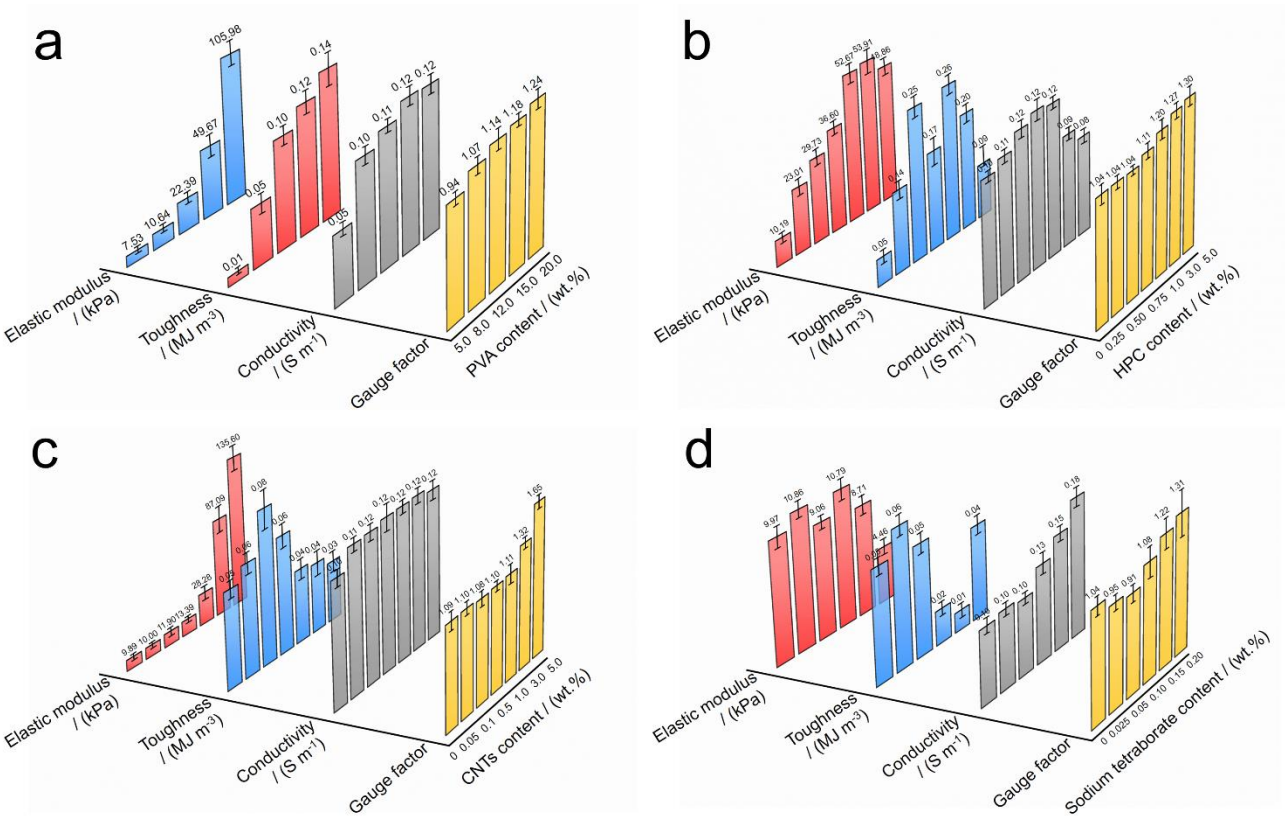

Supplementary Figure 1. One-component effect on PVA-based hydrogels. a The calculated mechanical and electrical properties of the pure PVA hydrogels with different weight percentages. By increasing the weight percentage of PVA, the elastic modulus and toughness increased obviously. **b** The calculated mechanical and electrical properties of the 8.0 wt.% PVA hydrogels with different HPC weight percentages. HPC content also can improve the modulus of PVA hydrogel, but excessive HPC decreases the maximum strain at break. **c** The calculated mechanical and electrical properties of the 8.0 wt.% PVA hydrogels with different CNTs weight percentages. The influence of CNTs on PVA hydrogel mainly reflects in the increase of the modulus and gauge factor, especially when the CNTs content over 1.0 wt.%. **d** The calculated mechanical and electrical properties of the 8.0 wt.% PVA hydrogels with different sodium tetraborate weight percentages. Sodium tetraborate can be hydrolyzed by the aqueous solution to yield boric acid/tetrafunctional borate ions. However, redundant boric acid could prevent the cross-linking of PVA, damaging its mechanical performances[1].

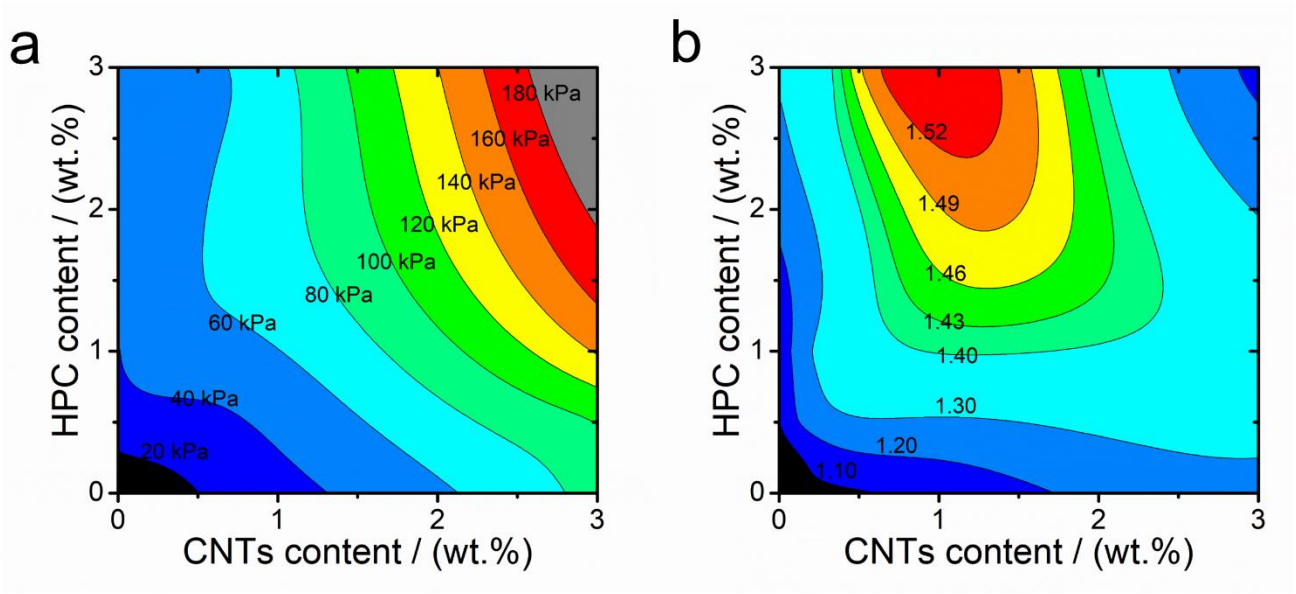

Supplementary Figure 2. Two-component effect on PVA-based hydrogels. a Elasticity modulus and **b** gauge factor mapping between various contents of HPC and CNTs. The results show that the elasticity modulus of the hybrid PVA hydrogel is associated with both HPC and CNTs contents. While the appropriate CNTs content contributes to the high gauge factor. CNTs act as conductive fillers in the hydrogel matrix. Parts of the resistance variation of hybrid PVA hydrogel are likely to the percolation theory.

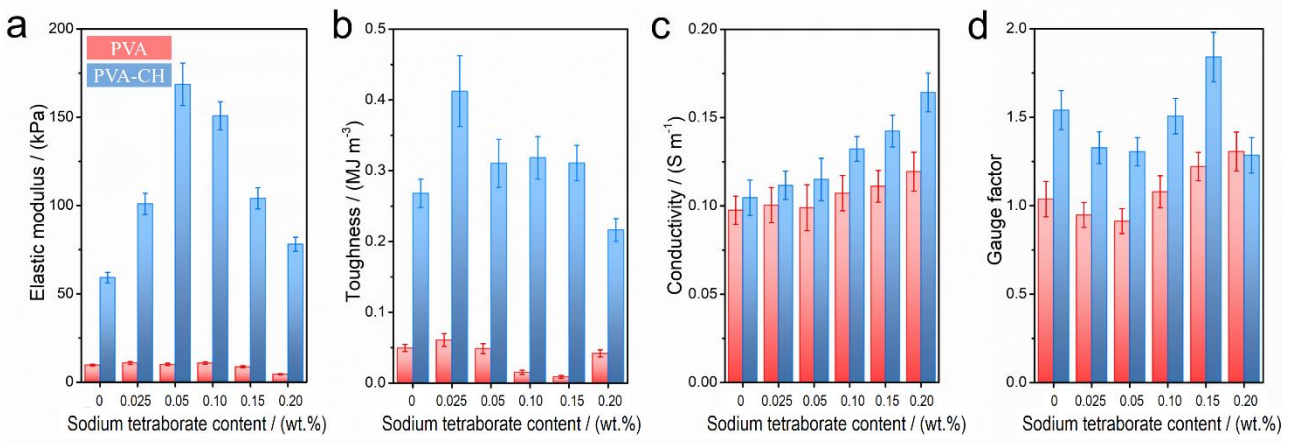

Supplementary Figure 3. The sodium tetraborate content effect on PVA-S hydrogels. a Elastic modulus, **b** toughness, **c** conductivity and **d** gauge factor of PVA-S hydrogels with different sodium tetraborate weight percentages from 0 to 0.20 wt.%. Some observations including: 1) Similar change variation tendency between PVA and PVA-CH of the four parameters vs. borax concentrations; 2) PVA-CH shows an order of magnitude stronger than PVA and slightly increased electronic responding.

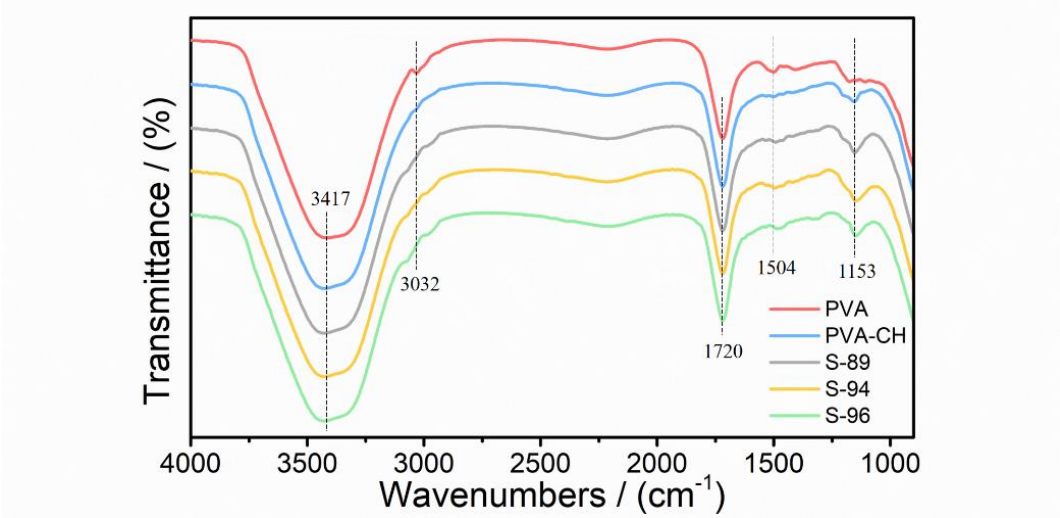

Supplementary Figure 4. FTIR spectra of representative PVA-S hydrogels. Table S1 gives the most characteristic bands of PVA and their respective assignment. All of the significant peaks of PVA hydrogel can be observed in all samples' FTIR spectra, which indicated that HPC/CNTs didn't interact with PVA, and no chemical reaction happened during the gelation process[2]. The broad and strong peak around 3400 cm^{-1} is attributed to the symmetrical stretching vibration of -OH groups which is sensitive to hydrogen bonding[3]. Compared with the physical crosslinking pure PVA, the peak shifts to a higher wavenumber indicates the presence of a certain amount of hydrogen bonding interactions between the hydroxyl groups on the PVA molecular chains and tetrafunctional borate ion. In addition, the degrees of crystallinity were obtained from the peak at ~1153 cm^{-1}. The intensity of this peak is influenced by the crystalline portion of the polymeric chains, which is dependent on the number of OH groups from the PVA[4].

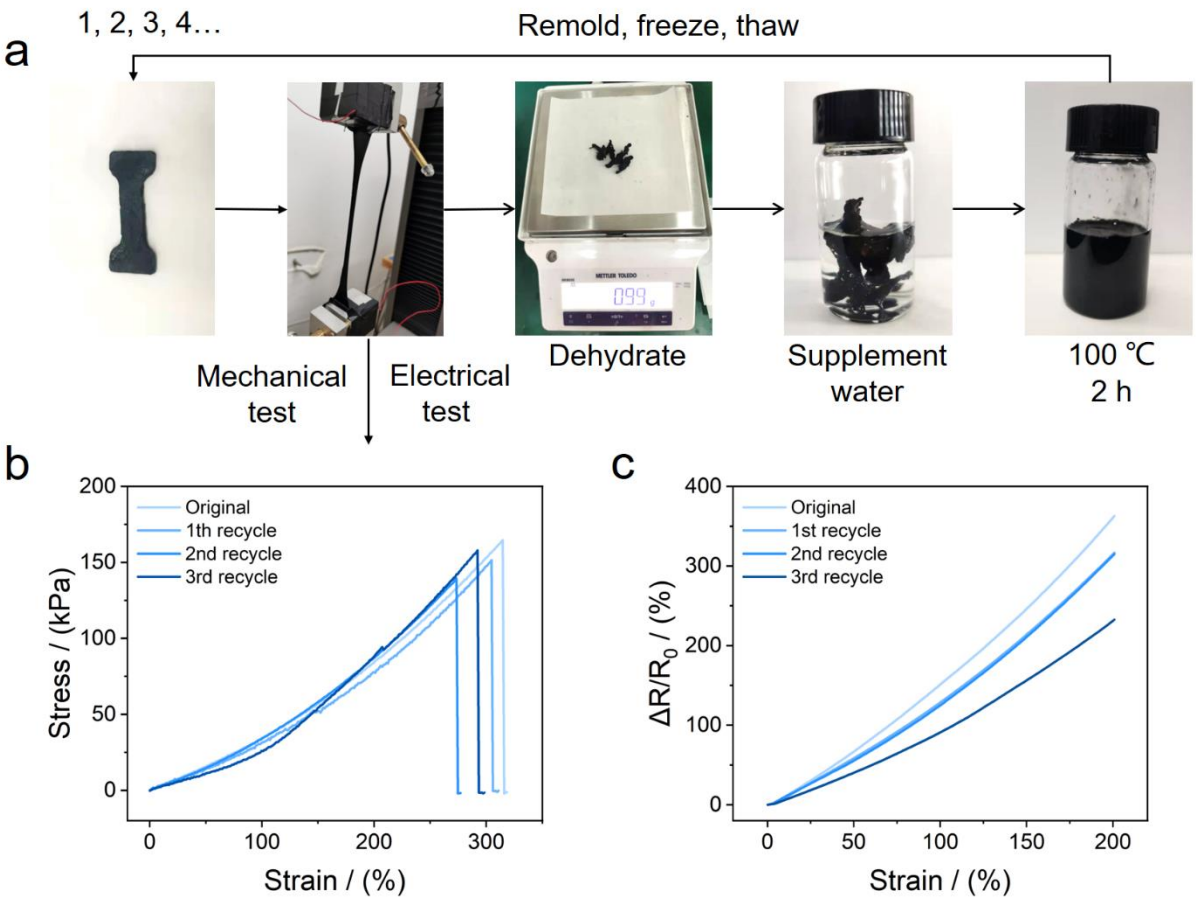

Supplementary Figure 5. Remoldability and reusability of PVA-S hydrogels. a Photographs of the remold process and mechanical test of the PVA-S hydrogels. **b** Tensile stress-strain curves and **c** electrical resistance variation curves of representative PVA-S hydrogels in 4 reversible remold process.

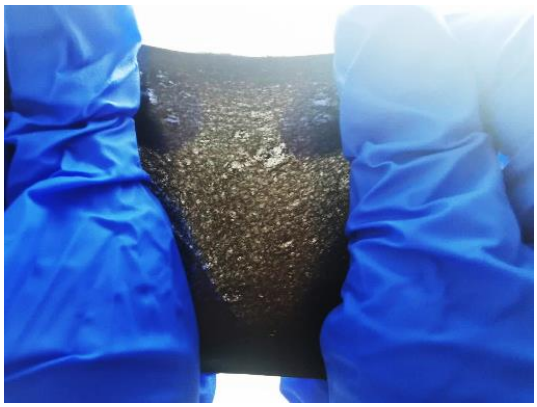

Supplementary Figure 6. Photograph of a PVA-S hydrogel after planar stretching. It presents abundant porous fiber networks.

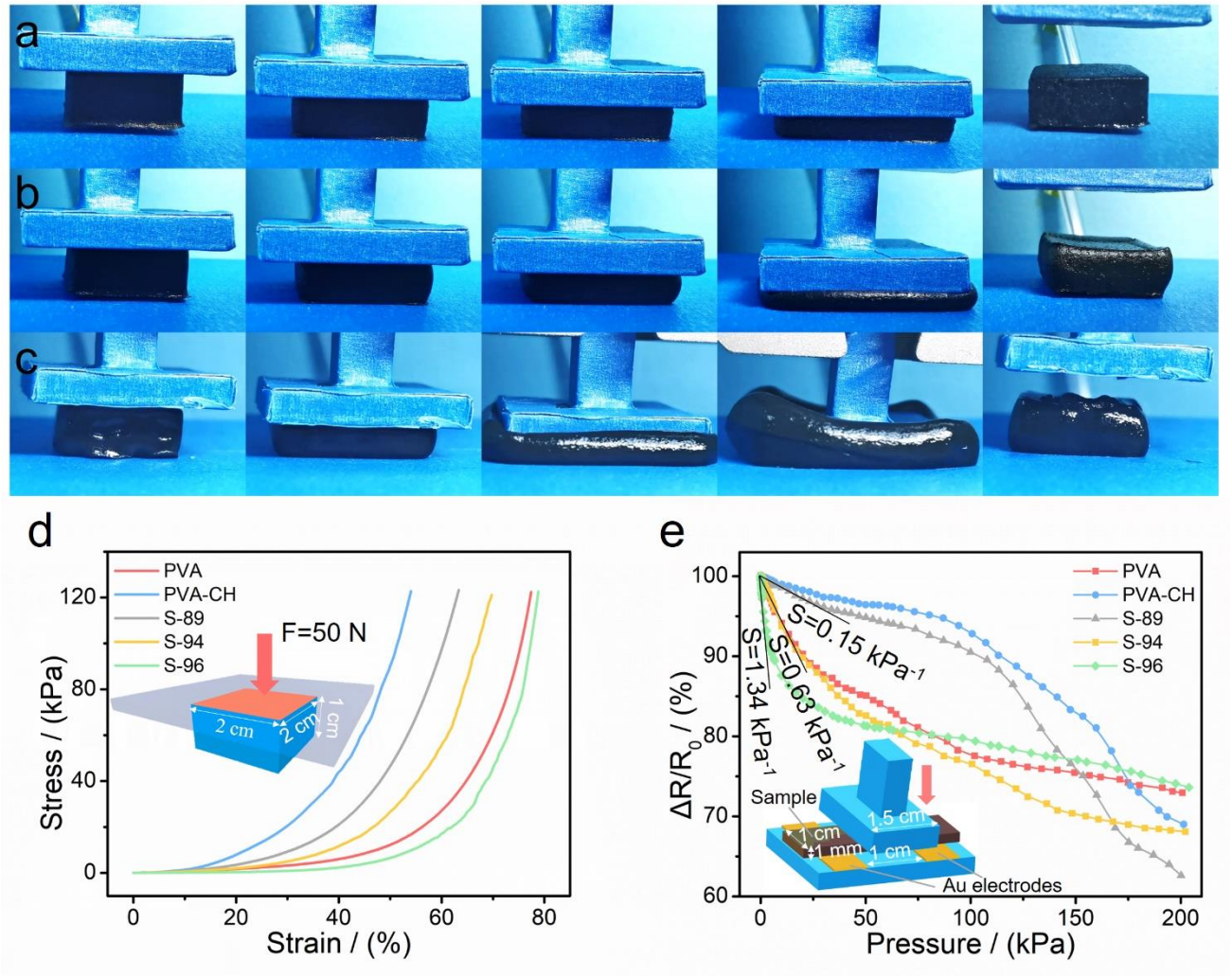

Supplementary Figure 7. Pressure measurement of representative hydrogels. Photographs of the **a** S-89, **b** S-94, and **c** S-96 hydrogels (2 cm×2 cm×1 cm) demonstrating their exceptional mechanical strength exhibited on 50 N compressive loading, and recovered immediately after removal of the force. **d** Compressive stress-strain curves for the representative hydrogels. **e** Resistance variation versus pressure for representative hydrogels. S-96 hydrogel shows the highest pressure sensitivity up to 1.34 kPa^{-1}. Inset describes the testing method.

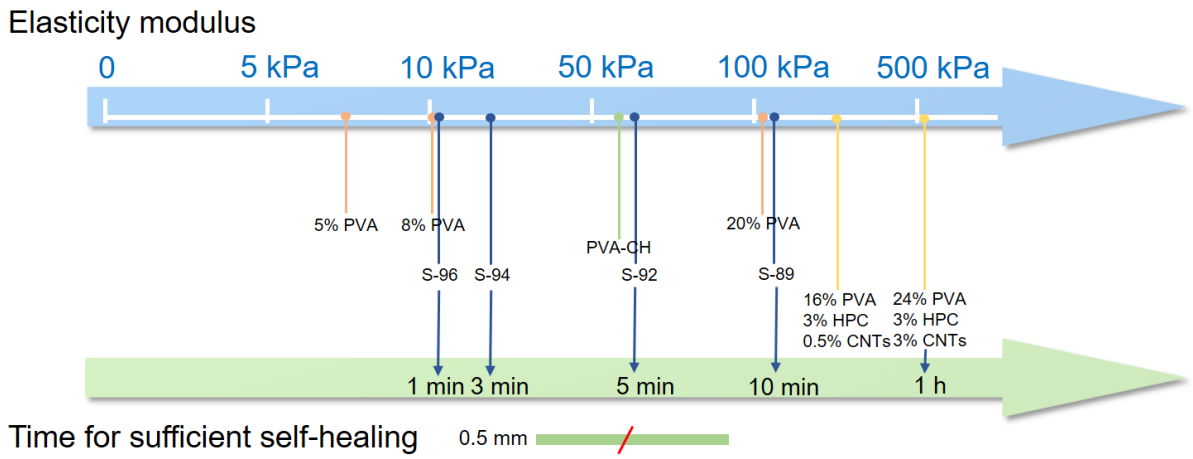

Supplementary Figure 8. Summary of elastic modulus and time for sufficient self-healing of the PVA-S hydrogels with different components. PVA-S hydrogels display a large tunable range of both elastic modulus and self-healing.

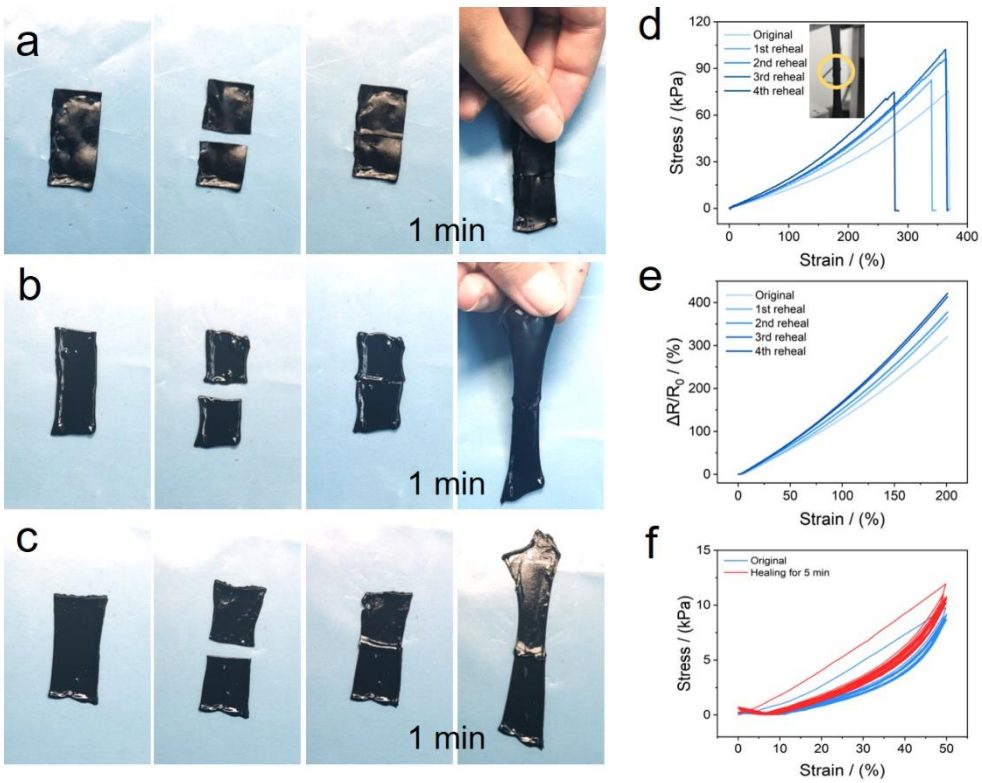

Supplementary Figure 9. Self-healing performance of representative PVA-S hydrogels. Photographs of the **a** S-89, **b** S-94, and **c** S-96 hydrogel films (4 cm×2 cm×1 mm) cut into two pieces and rejoined back into a rectangle, and then further undergoes a stretch after healing at 1 min. **d** Stress-strain curves, **e** electrical resistance variation curves and **f** twenty successive loading-unloading curves at a strain of 50% for original and healed S-94 hydrogel samples after 5 min healing.

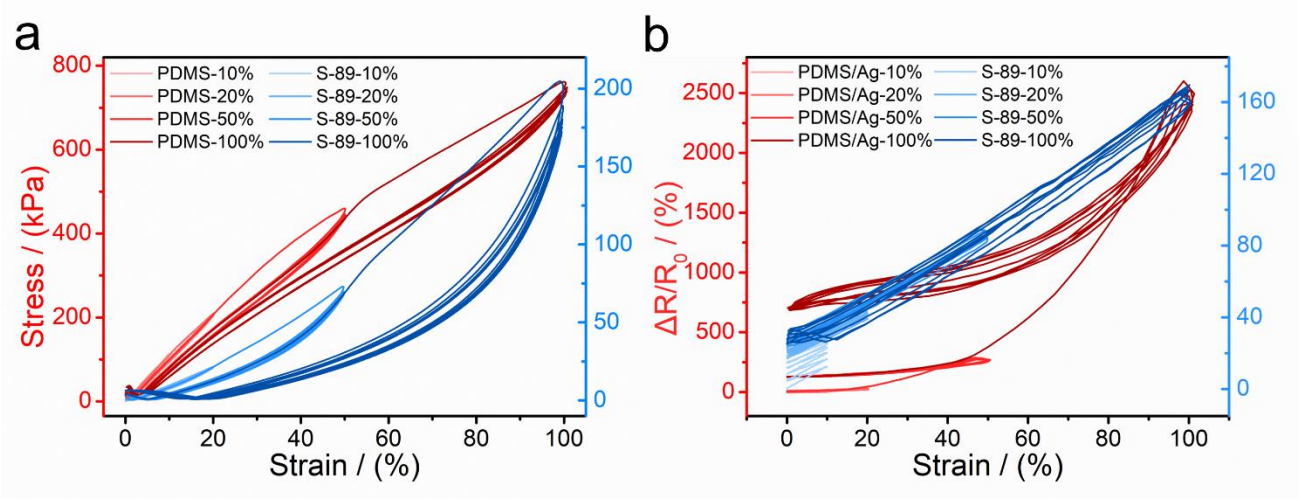

Supplementary Figure 10. Five successive cyclic tensile performances. a The loading-unloading curves of PVA-S hydrogel vs. PDMS at a strain of 10%, 20%, 50%, 100% with a continuous test, respectively. Comparing PDMS elastomer, S-89 shows larger hysteresis loops due to substantial bond scission. **b** The resistance variation-tensile curves of PVA-S hydrogel vs. PDMS/Ag micro-particles at a strain of 10%, 20%, 50%, 100% with a continuous test, respectively. For the electronic conductor, upon the first release of the strain, the resistance was just partially recovered when the PDMS was fully released[5].

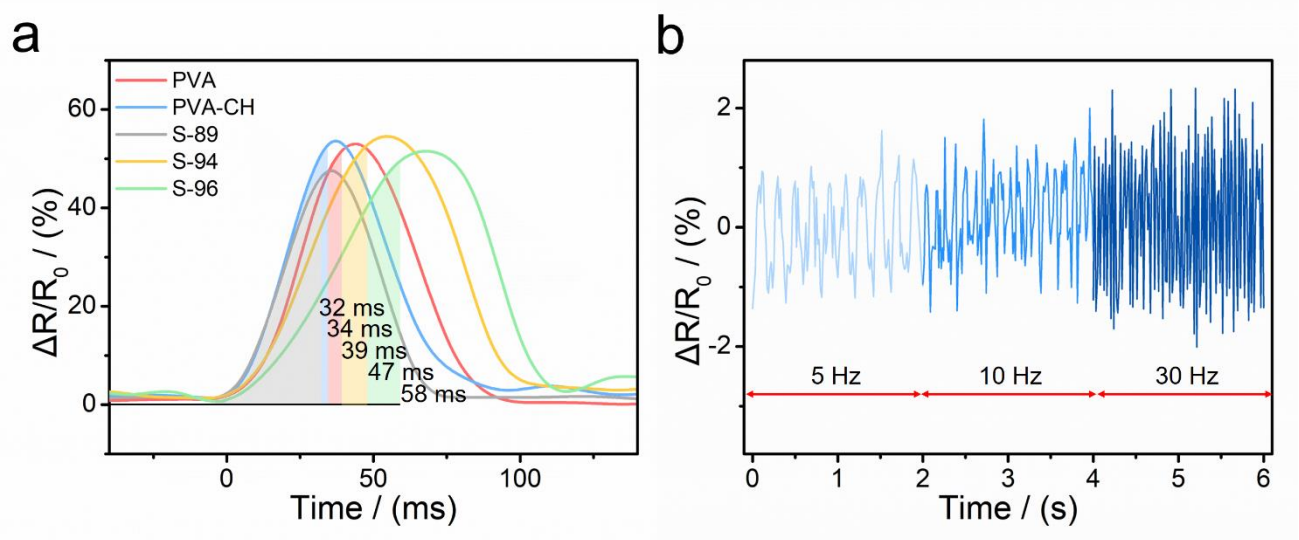

Supplementary Figure 11. Dynamic responding performance. a The response time of representative hydrogel samples under applied dynamical pressure. **b** The dynamical force responding curves of S-89 hydrogel.

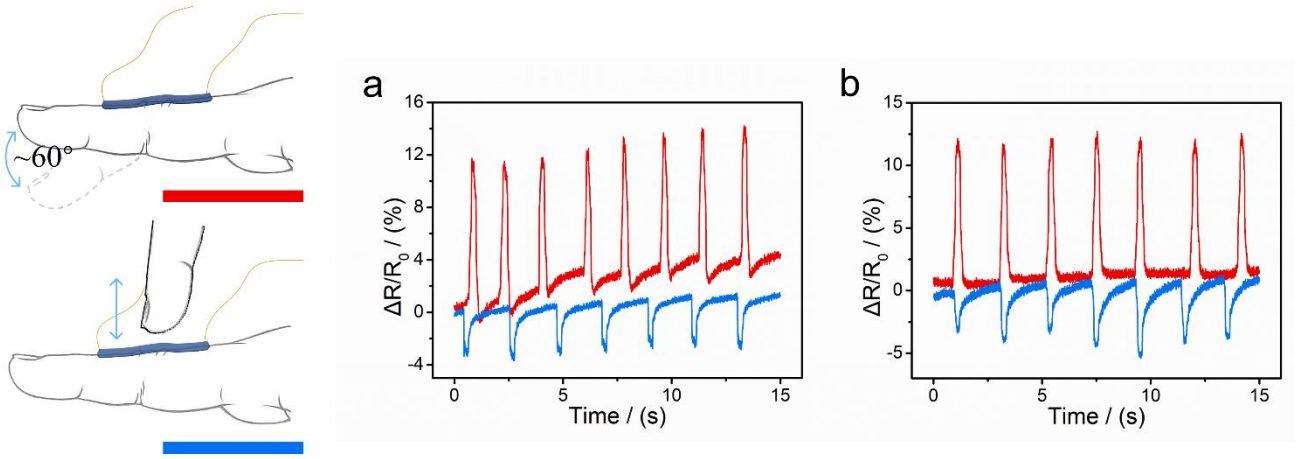

Supplementary Figure 12. Skin-attached sensing performance. a PVA and **b** PVA-S hydrogels were attached to a finger (without additional fixed) when the hand was bending and touched by another finger slightly, respectively. However, PVA-S hydrogel shows better signal stability due to the excellent skin adhesion performance and intrinsic electronic stability.

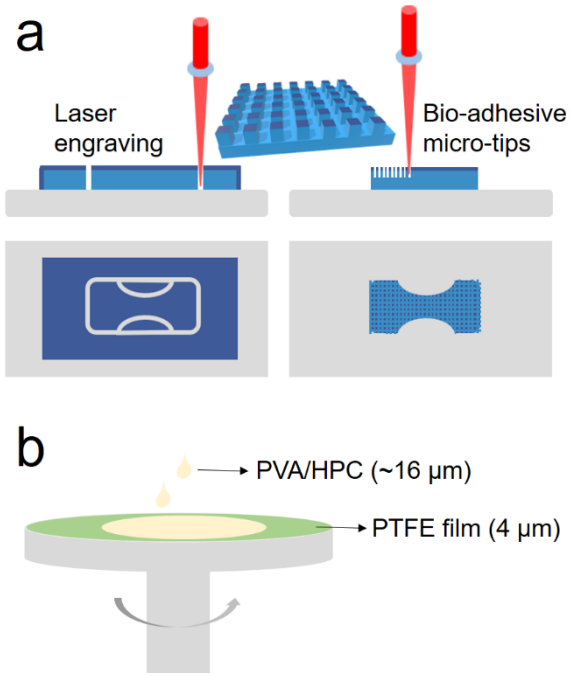

Supplementary Figure 13. The preparation process of hydrogel epidermis device. Schematic illustration of the fabrication process of skin-adhesive **a** PVA-S hydrogel electrode and **b** PP film. The selective laser engraving of a piece of PVA-S hydrogel to achieve patterns with processed micro-tips (300 μm) surface.

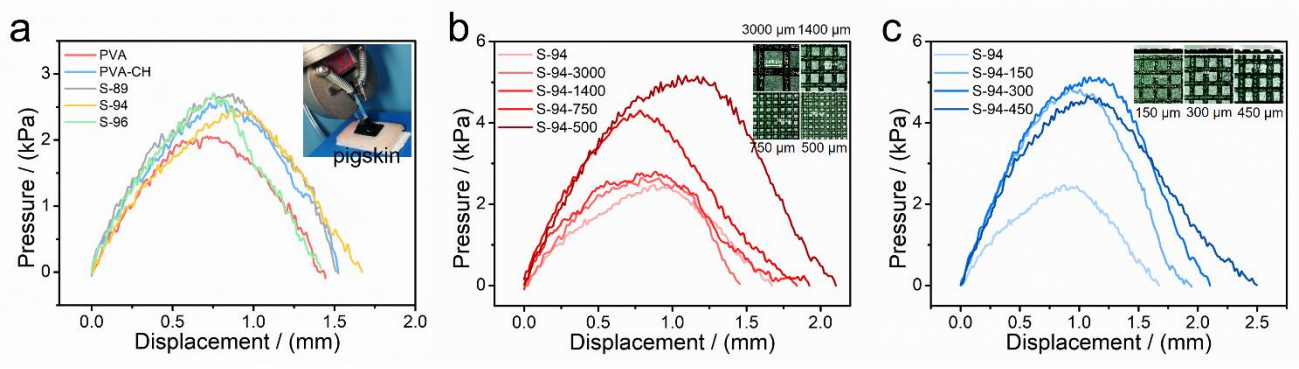

Supplementary Figure 14. Adhesion-force measurement. a Pressure-displacement curves of unstructured hydrogel samples and a photograph of PVA-S hydrogels attached to the pigskin during the adhesion experiment. **b** Pressure-displacement curves of S-94 with various microtip sizes. **c** Pressure-displacement curves of S-94 with various microtip depths.

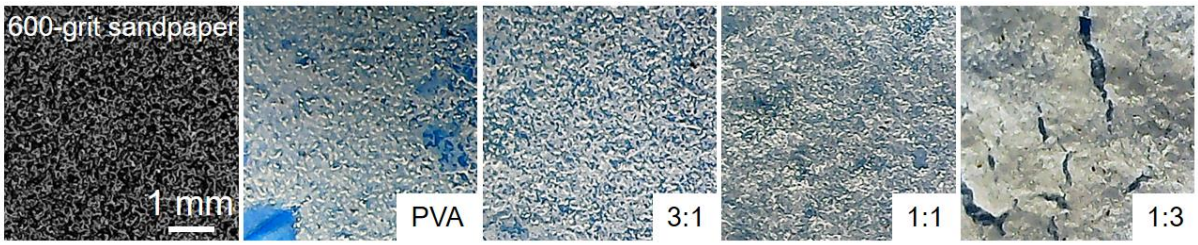

Supplementary Figure 15. Optical microscope characterization of the shape-adaptation performance of the PP films with different ratios of PVA:HPC. It is difficult to build enough accumulated matrix to achieve conformality for the water-soluble pure PVA sample on a 600-grit sandpaper substrate with random microscale surface roughness. While a large proportion of HPC results in the inferior diffusion of the sticky medium.

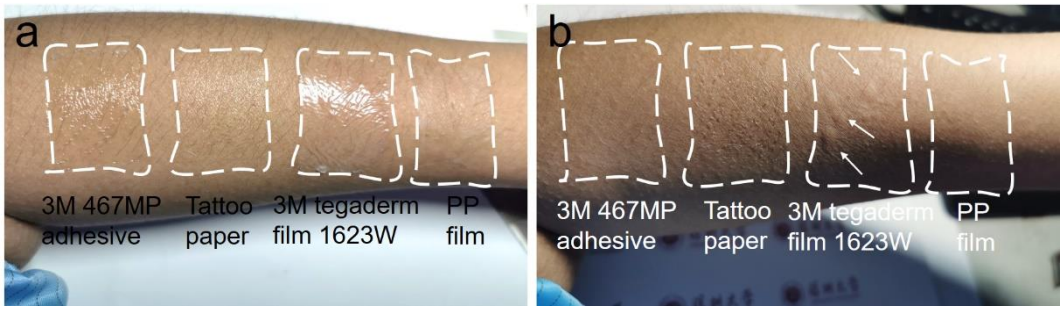

Supplementary Figure 16. Biocompatibility test of the PP film. a 3M 467MP adhesive, tattoo paper, 3M tegaderm film 1623W, and PP film were attached to the forearm for 6 h. **b** Comparison of the commercial patch and tattoo paper, the PP film without leaving a sticky remnant (3M 467MP adhesive and tattoo paper) or causing an inflammatory response (3M tegaderm film 1623W) during/after peeling.

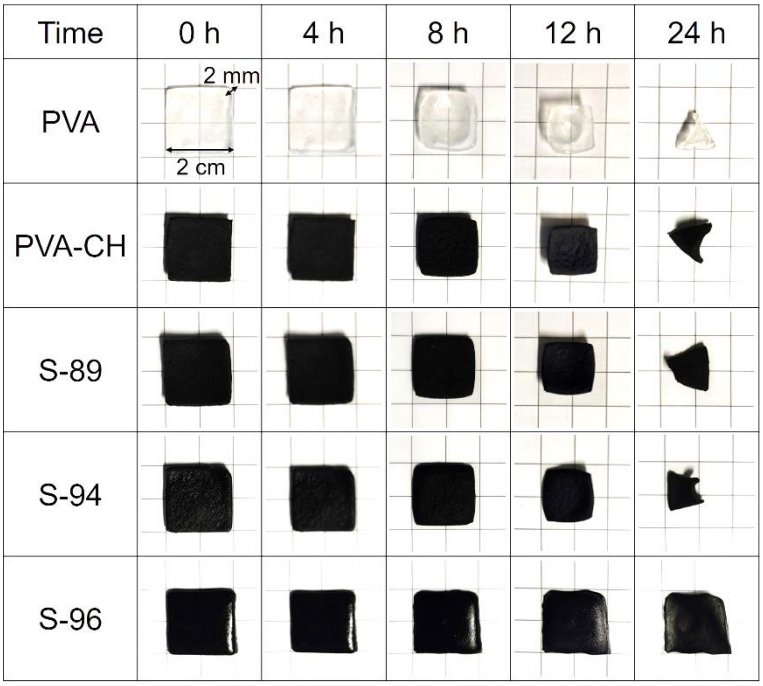

Supplementary Figure 17. The water retentiveness of PVA-S hydrogels. Images of the representative hydrogels after placed in air for 4 h, 8h, 12 h, 24 h, respectively.

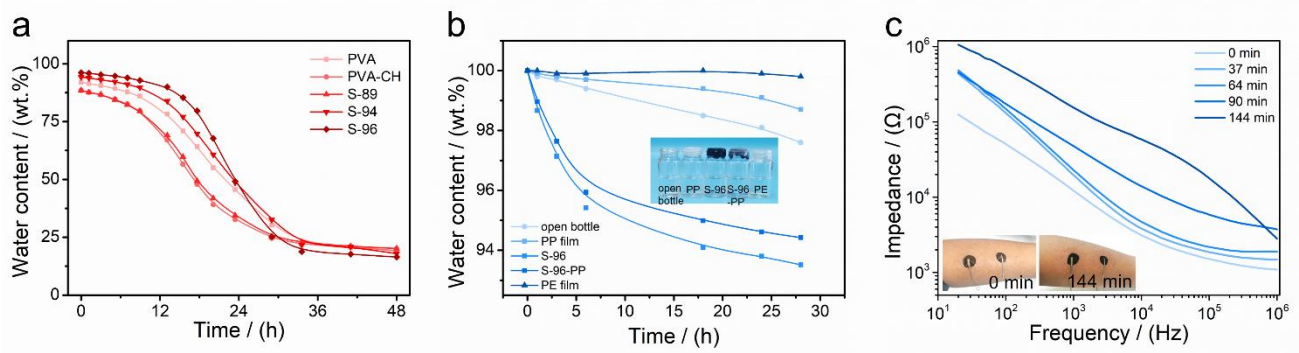

Supplementary Figure 18. The water retentiveness and long-lasting electronic performance of PVA-S hydrogels. a The water content of the representative hydrogels as a function of time. **b** Water-vapor rate of the representative samples as a function of time. Inset describes the experimental setup. The initial dropping of the S-96 and S-96-PP is due to the dehydration of PVA-S hydrogel. It indicates that PP film and PHEE exhibit available water-vapor permeability. **c** The electrode-skin impedance of PHEE as a function of time.

Supplementary Table 1. Vibration modes and band frequencies in PVA.

Wavenumber / (cm^{-1})	Chemical group
3417	O-H stretching vibration from the intermolecular and intramolecular hydrogen bonds
3032	C-H from alkyl groups
1720	C=O and C-O from acetate group
1504	CH_2 bending
1153	C-O-C

Supplementary Table 2. Compared water content, elastic modulus of representative self-healing hydrogels and polymers reported in recent 5 years.

Category	Material	Water content	Elastic Modulus	Healing time	Healing condition	Ref.
PVA Hydrogel	**PVA-S**	**70-96 wt.%**	**10-500 kPa**	**1-60 min**	**R. T.**	**This work**
	PVA-PDA[a)]	≈90 wt.%	≈5 kPa	250 ms	R. T.	6
	PVA/SWCNT[b)]	≈96 wt.%	/	3.2 s	R. T.	1
	PVA-agarose	≈78 wt.%	5-15 kPa	10-60 s	R. T.	7
	PVA-NAGA[c)]	≈88 wt.%	≈100 kPa	2 h	R. T.	8
	PVA-PAA[d)]	≈90 wt.%	≈15 kPa	6 h	R. T.	9
	PVA	65 wt.%	≈40 kPa	48 h	R. T.	10
	PVA/ PEDOT:PSS[e)]	/	14-330 kPa	/	heated to 80 °C and reduced to -20 °C	11
	PVA-CNT	80%-95%	1-25 kPa	/	Applying repairing solutions	12
	PVA-PAM[f)]	≈87 wt.%	62 kPa	∞	/	13
	PVA-HPC	≈84 wt.%	590 kPa	∞	/	2
	PVA exogel	≈82 wt.%	≈100 kPa	∞	/	14
Hydrogel	PDA[g)]/Ag NPs[h)]	≈90 wt.%	132 Pa-40 kPa	2 h	R. T.	15
	PDA-pGO[i)]-PAM	80 wt.%	≈6 kPa	1 d	R. T.	16
	PAA-chitosan-MBAA[j)]	≈97 wt.%	≈1-4 kPa	180 s	R. T.	17
	Poly(MAA[k)]-co-OEGMA[l)])	≈60-80 wt.%	650 kPa-4.3 MPa	40 min	R. T.	18
Polymer	PDMS-MPU[m)]-IU[n)]	0	0.7 MPa	12 h	under water	19
	CB[8][o)]-Am[p)]	/	≈1 MPa	12 h	R. T.	20
	TPU[q)]	0	≈1 MPa	2 h	R. T.	21
	Cu-DOU-CPU[r)]	0	≈14 MPa	130 h	R. T.	22
	PAA-PVPON[s)]	≈5.9 wt.%	≈81 MPa	11 h	in water at 45 °C	23

[a)] PDA: polydopamine; [b)] SWCNT: single wall carbon nanotube; [c)] NAGA: N-acryloyl glycinamide; [d)] PAA: polyacrylic acid [e)] PEDOT:PSS: poly(3,4-ethylenedioxythiophene):polystyrene sulfonate; [f)] PAM: polyacrylamide; [g)] PDA: polydopamine; [h)] Ag NPs: silver nanoparticles; [i)] pGO: partially reduced graphene oxide; [j)] MBAA: N,N″-methylenebis-acrylamide; [k)] MAA: methacrylic acid; [l)] OEGMA: oligo(ethyleneglycol) methacrylate; [m)] MPU: 4,4′-methylenebis(phenylurea); [n)] IU: isophorone bisurea units; [o)] CB[8]: cucurbit[8]uril; [p)] AM: acrylamide; [q)] TPU: thermoplastic polyurethane; [r)] Cu-DOU-CPU: Cu-dimethylglyoxime-urethane-covalently cross-linked polyurethane; [s)] PVPON: polyvinylpyrrolidone

Due to there are differences in test methods of various papers, and lacking sufficient data to normalize it, so these results are for reference only.

Supplementary Movie 1. Stretching the PVA-S manually. Demonstration of the resilient, self-healing, and porous nature of PVA-S hydrogel simultaneously by lifting a metal ring (600 g).

Supplementary Movie 2. Various kinds of deformations to PHEE. A video of the compressed and stretched deformations as well as the skin-friendly removal process of PHEE.

Supplementary Movie 3. Demo of AR based on PHEE. Demonstration of playing the game (3D Pinball) controlled by multi-channel EMG signals collected by PHEE.

Supplementary References

1. Cai, G. et al. Extremely stretchable strain sensors based on conductive self-healing dynamic cross-links hydrogels for human-motion detection. *Adv. Sci.* **4**, 1600190 (2017).
2. Zhou, Y. et al. Highly stretchable, elastic, and ionic conductive hydrogel for artificial soft electronics. *Adv. Funct. Mater.* **29**, 1806220 (2019).
3. Kale, S. et al. Intramolecular and intermolecular crosslinked poly (vinyl alcohol)-borate complexes for the sustained release of fertilizers and enzymes. *J. Appl. Polym. Sci.* **121**, 2450-2457 (2011).
4. Mansur, H. S. Sadahira, C. M. Souza, A. N. & Mansur, A. A. FTIR spectroscopy characterization of poly (vinyl alcohol) hydrogel with different hydrolysis degree and chemically crosslinked with glutaraldehyde. *Mater. Sci. Eng. C* **28**, 539-548 (2008).
5. Xu, F. & Zhu, Y. Highly conductive and stretchable silver nanowire conductors. *Adv. Mater.* **24**, 5117-5122 (2012).
6. Liu, S. et al. A compliant, self-adhesive and self-healing wearable hydrogel as epidermal strain sensor. *J. Mater. Chem. C* **6**, 4183-4190 (2018).
7. Chen, W.-P. et al. Hydrogel with ultrafast self-healing property both in air and underwater. *ACS Appl. Mater. Interfaces* **10**, 1258-1265 (2018).
8. Ma, M. et al. A facile strategy for synergistic integration of dynamic covalent bonds and hydrogen bonds to surmount the tradeoff between mechanical property and self-Healing capacity of hydrogels. *Macromol. Mater. Eng.* **306**, 2000577 (2020).
9. Ge, G. et al. Highly stretchable and autonomously healable epidermal sensor based on multi-functional hydrogel frameworks. *J. Mater. Chem. A* **7**, 5949-5956 (2019).
10. Zhang, H. Xia, H. & Zhao, Y. Poly (vinyl alcohol) hydrogel can autonomously self-heal. *ACS Macro Lett.* **1**, 1233-1236 (2012).
11. Rong, Q. et al. Anti-freezing, conductive self-healing organohydrogels with stable strain-sensitivity at subzero temperatures. *Angew. Chem. Int. Edi.* **56**, 14159 (2017).
12. Wang, H. et al. A highly elastic, room-temperature repairable and recyclable conductive hydrogel for stretchable electronics. *J. Colloid Interf. Sci.* **588**, 295-304 (2021).

13. Ge, G. et al. Stretchable, transparent, and self-patterned hydrogel-based pressure sensor for human motions detection. *Adv. Funct. Mater.* **28**, 1802576 (2018).
14. Xu, L. et al. A solvent-exchange strategy to regulate noncovalent interactions for strong and antiswelling hydrogels. *Adv. Mater.* **32**, 2004579 (2020).
15. Zhao, Y. et al. Skin-inspired antibacterial conductive hydrogels for epidermal sensors and diabetic foot wound dressings. *Adv. Funct. Mater.* **29**, 1901474 (2019).
16. Han, L. et al. A mussel-inspired conductive, self-adhesive, and self-healable tough hydrogel as cell stimulators and implantable bioelectronics. *Small* **13**, 1601916 (2017).
17. Darabi, M. A. et al. Skin-inspired multifunctional autonomic-intrinsic conductive self-healing hydrogels with pressure sensitivity, stretchability, and 3D printability. *Adv. Mater.* **29**, 1700533 (2017).
18. Jiang, Z. Diggle, B. Shackleford, I. C. & Connal, L. A. Tough, self-healing hydrogels capable of ultrafast shape changing. *Adv. Mater.* **31**, 1904956 (2019).
19. Kang, J. et al. Tough and water-insensitive self-healing elastomer for robust electronic skin. *Adv. Mater.* **30**, 1706846 (2018).
20. Liu, J. et al. Tough supramolecular polymer networks with extreme stretchability and fast room-temperature self-healing. *Adv. Mater.* **29**, 1605325 (2017).
21. Kim, S. M. et al. Superior toughness and fast self-healing at room temperature engineered by transparent elastomers. *Adv. Mater.* **30**, 1705145 (2018).
22. Zhang, L. et al. A highly efficient self-Healing elastomer with unprecedented mechanical properties. *Adv. Mater.* **31**, 1901402 (2019).
23. An, N. et al. Healable and mechanically super-strong polymeric composites derived from hydrogen-bonded polymeric complexes. *Adv. Mater.* **31**, 1904882 (2019).